Self-powered electrochemical system by combining Fenton reaction and active chlorine generation for organic contaminant treatment

Yawei Feng[1,2,§], Kai Han[1,2,§], Tao Jiang[1,2,§], Zhenfeng Bian[3], Xi Liang[1,2], Xia Cao[1,2] (✉), Hexing Li[4] (✉), and Zhong Lin Wang[1,2,5] (✉)

[1] *CAS Center for Excellence in Nanoscience, Beijing Key Laboratory of Micro-nano Energy and Sensor, Beijing Institute of Nanoenergy and Nanosystems, Chinese Academy of Sciences, Beijing 100083, China*

[2] *School of Nanoscience and Technology, University of Chinese Academy of Sciences, Beijing 100049, China*

[3] *Education Ministry Key and International Joint Lab of Resource Chemistry and Shanghai Key Lab of Rare Earth Functional Materials, Shanghai Normal University, Shanghai 200234, China*

[4] *School of Environmental and Chemical Engineering, Shanghai University of Electric Power, Shanghai 200090, China*

[5] *School of Material Science and Engineering, Georgia Institute of Technology, Atlanta, GA 30332, USA*

[§] *Yawei Feng, Kai Han, and Tao Jiang contributed equally to this work.*

ABSTRACT

Environmental deterioration, especially water pollution, is widely dispersed and could affect the quality of people's life at large. Though the sewage treatment plants are constructed to meet the demands of cities, distributed treatment units are still in request for the supplementary of centralized purification beyond the range of plants. Electrochemical degradation can reduce organic pollution to some degree, but it has to be powered. Triboelectric nanogenerator (TENG) is a newly-invented technology for low-frequency mechanical energy harvesting. Here, by integrating a rotary TENG (R-TENG) as electric power source with an electrochemical cell containing a modified graphite felt cathode for hydrogen peroxide (H_2O_2) along with hydroxyl radical (•OH) generation by Fenton reaction and a platinum sheet anode for active chlorine generation, a self-powered electrochemical system (SPECS) was constructed. Under the driven of mechanical energy or wind flow, such SPECS can efficiently degrade dyes after power management in neutral condition without any O_2 aeration. This work not only provides a guideline for optimizing self-powered electrochemical reaction, but also displays a strategy based on the conversion from distributed mechanical energy to chemical energy for environmental remediation.

KEYWORDS

self-powered electrochemistry, Fenton reaction, active chlorine, organic contaminant degradation

1 Introduction

Distributed mechanical energy from wind blow, water flow, animal motion and human action, is widely existed around. Triboelectric nanogenerator (TENG) is a newly-invented technology for low-frequency mechanical energy harvesting at a high efficiency [1, 2]. By coupling of triboelectrification and electrostatic induction, mechanical vibration or relative displacement of metal electrode and dielectric materials can be converted into electricity [3, 4]. This electricity generation origins from Maxwell's displacement current, which is essentially different from traditional electromagnetic generator [5, 6]. The efficient conversion by TENGs makes it possible to power light-emitting diodes, wireless transmitters, sensors, even to realize the world of internet of things [7, 8]. The design of TENGs is rather flexible due to the utilization of various dielectric and conductive materials, which have found applications in the fields of tribotronics, self-powered systems and hybrid energy harvesting devices [9–12]. The electric energy translated from TENGs can also be used in electrochemistry and photo-electrochemistry [13–16]. For example, efficient self-powered water splitting can be directly realized at a rate of 6.25×10^{-3} mL/min by integrating an electrolysis cell and flowing-water-driven TENG [17]. Assisted with the induced electric

field, photocatalytic hydrogen generation and organic compounds degradation in aqueous condition can be significantly promoted [18–20]. An insulating featured photocatalyst-loaded electrostatic filter can achieve a doubled efficiency of gaseous formaldehyde degradation, when a peak voltage of 1,110 V is applied on the filter by a single electrode TENG [21].

On the other hand, environmental deterioration, especially water pollution, is widely dispersed [22, 23]. Though the sewage treatment plants are used to meet the demands of cities, distributed treatment units are still in request for the supplementary of centralized purification beyond the range of plants. Electro-Fenton (EF) reaction, a derivatived advanced oxidation processes from Fenton reaction and electrochemistry, is widely used for organic contaminant treatment [24, 25]. The main reactions are hydrogen peroxide (H_2O_2) electro-generation over cathode and decomposition under the catalytic effect of Fe^{2+} ions, forming hydroxyl radical (•OH), along with the regenation of Fe^{2+} ions through Fe^{3+} reduction on cathode [24, 26, 27]. •OH is a kind of active oxygen species with higher oxidation potential ($E^0_{(•OH,H^+/H_2O)} = 2.72$ V), than the standard one of ozone under acidic conditions [28, 29]. The traditional EF process is conducted by an extra power source in an electrochemical cell, thus electric circuit design needs to be considered for large-scale application

Address correspondence to Zhong Lin Wang, zhong.wang@mse.gatech.edu; Hexing Li, hexing-li@shnu.edu.cn; Xia Cao, caoxia@binn.cas.cn

outdoors. Hence, EF process powered by distributed energy source, such as wind blow or water flow, is more prospective for the applications in the water area beyond the sewage treatment plants. Besides, electrolyte is needed for electric conductivity enhancement in the aqueous phase. Chloride-based salt electrolyte can produce active chlorine species, like hypochlorous (HClO), hypochlorite ion (ClO$^-$), via dissolving the evolved chlorine (Cl$_2$) in aqueous solution [30, 31]. The generated active chlorine species can also contribute to the degradation of organic compounds coordinated with •OH species generated in the EF process.

In this work, a self-powered electrochemical system (SPECS) was constructed by a rotary TENG (R-TENG) driving electrochemical cell for the generation of H$_2$O$_2$, •OH and active chlorine species. Modified graphite felt (GF) cathode with mesoporous carbon black and polytetrafluoroethylene (PTFE) nanopowder was prepared, which can efficiently generate H$_2$O$_2$ by making full use of dissolved oxygen (O$_2$) in neural condition. Platinum sheet was used as the anode for the generation of active chlorine species. With power management, this constructed SPECS can efficiently degrade Rhodamine B (RhB) and methylene blue (MB) in neutral condition without any O$_2$ aeration and external electric power supply. A wind-driven rotary TENG (WR-TENG) was also fabricated for the demo application of SPECS. The SPECS presented in this work would not only extend the application of TENGs in electrochemistry, but also provide a promising strategy for the treatment of distributed water pollution via the conversion from distributed mechanical energy to chemical energy.

2 Experimental section

2.1 Fabrication of the R-TENG

The R-TENG consists of two well fixed coaxial parts. For the stator, 1 oz Cu was deposited on a disk-shape printed circuit board (PCB). The whole PCB was divided into 12 intervals for Cu electrode deposition, and gaps were reserved between the neighboring electrodes. For the rotator, the FR4 glass fiber board (1 mm in thickness) was cut into the same size as the effective contact area of stator (20 cm for external diameter, 4 cm for internal diameter). A 50 μm-thick Kapton film was cut into annular sector shape, which was closely adhered onto the FR4 board at intervals. A motor was used to trigger the rotator for rotation movement, and a transmission was used for adjusting the rotational condition. The open-circuit voltage (V_{OC}), transferred charge (Q_{SC}) and short-circuit current (I_{SC}) outputs were measured by Keithley 6514 system electrometer.

2.2 Preparation of cathode electrode

Graphite felt (GF, 3 mm in thickness) was cut into the size of 2 cm × 2.5 cm. Before modification, these felts were immersed in the mixture of acetone, alcohol and ultrapure water for ultrasonic cleaning, then dried at 80 °C. For the modification of graphite felt [32], 0.3 g mesoporous carbon black, 0.9 g nano-sized PTFE powder, 30 mL ultrapure water and 2 mL n-butanol were mixed under stirring for 40 min to form a dispersed suspension. The cleaned graphite felts were immersed into the above suspension under magnetic stirring for 30 min for the loading of carbon black and PTFE. After drying at 80 °C for 12 h, the felts were annealed at 360 °C for 1 h at a heating rate of 6 °C/min. The modified graphite felt was marked as GF-3, and the raw graphite felt was marked as GF-0.

2.3 Electrochemical characterization

The morphology of cathode was characterized using scanning electron microscopy (SEM, Nova NanoSEM 450 and Hitachi SU8020). Electrochemical characterization of the raw and modified graphite felts was performed on an electrochemical workstation (CHI660E)

in the three-electrode system. Linear sweep voltammetry (LSV) was recorded at a scanning rate of 10 mV/s. The modified graphite felt was used as cathode electrode, a platinum sheet (10 mm × 20 mm × 0.1 mm) as counter electrode and an Ag/AgCl electrode as reference electrode. NaCl aqueous solution (0.1 M) with or without Fe^{2+} ions (0.2 mM FeSO$_4$) was used as electrolyte.

2.4 Generation and measurement of H$_2$O$_2$ and •OH

The electro-generation of H$_2$O$_2$ was carried out in a single chamber cell (100 mL) at 22 °C. In this process, direct current (DC) was applied by Keithley 2410 SourceMeter, platinum sheet was used as the anode electrode, 50 mL of 0.1 M NaCl aqueous solution was used as the electrolyte, and constant stirring was employed for the diffusion of the generated H$_2$O$_2$. The pH value of electrolyte was adjusted by H$_2$SO$_4$ or NaOH, N$_2$ or O$_2$ was introduced at a flow rate of 0.6 L/min to determain the effect of atmosphere. At an interval of 2 min, 1 mL solution was pipette out for the quantitative detection of H$_2$O$_2$. The analysis method was referenced to spectrophotometric determination (Shimadzu UV3600) using titanium reagent (20 mM potassium titanium(IV) oxalate, 1 M sulphuric acid) [33]. •OH generated from H$_2$O$_2$ via Fenton process (0.2 mM FeSO$_4$) was quantitatively measured by determination of the fluorescence intensity (Edinburgh instruments, FLS980-S2S2-stm) of 2-hydroxyterephthalic acid evolved from hydroxylated terephthalic acid [34].

2.5 Degradation of RhB and MB

The degradation tests of RhB and MB were carried out in the same chamber cell as the H$_2$O$_2$ electro-generation. 0.1 M NaCl aqueous solution with 0.2 mM FeSO$_4$ was used as the electrolyte. The electrolyte solution was neutral. DC current (Keithley 2410 SourceMeter) or R-TENG was used as power source for the degradation. The concentration of RhB or MB dye was determined by spectrophotometer (Shimadzu UV 3600) at the characteristic absorption peak. The removal rate η was calculated by $\eta = 1 - (A_t/A_0)$, where A_t denotes the absorption intensity at the given time, and A_0 denotes the original intensity. The total organic carbon (TOC) content was determined by the combustion method on Shimadzu TOC-VCPN.

3 Results and discussion

3.1 Performance of R-TENG

Electricity generation of TENG originates from Maxwell's displacement current. The working principle of R-TENG is sketched in Fig. 1(a) and its structural design is illustrated in Fig. 1(b). FR4 glass fiber board adhered with Kapton layer acts as the rotator and PCB deposited with Cu layer acts as the stator for the R-TENG. When the dielectric Kapton layer contacts well with the bottom Cu electrode, negative charges are acquired. While the top dielectric layer spans the left and right Cu electrodes by rotation, the total negative polarization intensity above the right Cu electrode decreases, thus leading to the electron flow from the left to the right electrode through the external load circuit to screen the exceeding positive charges (stages (i) to (iii) in Fig. 1(a) and Fig. S1 in the Electronic Supplementary Material (ESM)). Continuing rotating to stage (iv), the negative polarization intensity decreases above the left electrode but increases above the right one, resulting in the backward flow of electrons from the right electrode to the left one. The rotation of Kapton layer in cycles drives electrons flow in the external load circuit for generating electricity.

The electrical output performance of the fabricated R-TENG is summarized in Figs. 1(c)–1(e). Since the charge density on the surface of Kapton is stable when it is saturated, the transferred charge in one cycle and induced voltage between two Cu electrodes are independent of the rotational speed of rotator, while the output
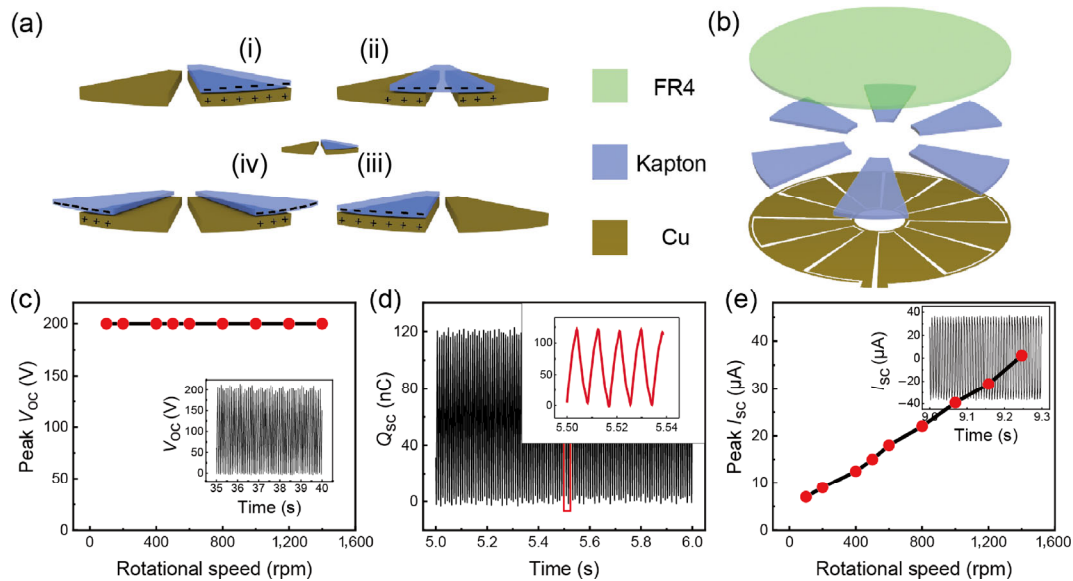
Figure 1 Schematic images and electrical output performance of R-TENG. (a) Working mechanism and (b) structural illustration of the fabricated R-TENG. (c) The peak V_{OC} of the R-TENG at different rotational speeds. The insert is the specific V_{OC} output at 400 rpm. (d) The Q_{SC} of the R-TENG at 1,200 rpm. The insert is the enlarged view inside the rectangle part. (e) The peak I_{SC} of the R-TENG at different rotational speeds. The insert is the specific I_{SC} output at 1,400 rpm.

current rises with increasing the rotational speed. As shown in Figs. 1(c) and 1(d), a peak V_{OC} of 200 V and a Q_{SC} of 120 nC are obtained, and the peak values are almost unchanged from 100 to 1,400 revolutions per minute (rpm). The I_{SC} really matters to the rotation speed, the measured peak value almost increases linearly with the rotational speed (Fig. 1(e)).

3.2 Characterization and electrochemical performance

For the construction of SPECS, cathode for high-efficiency generation of H_2O_2 and anode for active chlorine species are required. The raw GF acts as a three-dimensional (3D) supporter for the loading of electrocatalyst, mesoporous carbon black was chosen as the main catalytic component and PTFE nanopowder as co-catalytic component and binder. Though there is no notable difference in visual (Fig. S2 in the ESM), the amplified surface morphologies of GF before and after modification (Figs. 2(a) and 2(b)) are distinguishable. The loaded components fill the gaps of GF fibers (Figs. 2(b) and 2(c)), while the raw GF electrode (GF-0) is clean fiber structure with the diameter of 20 μm (Fig. S3 in the ESM). Though PTFE is also active for H_2O_2 generation, too much PTFE makes the as-prepared cathode
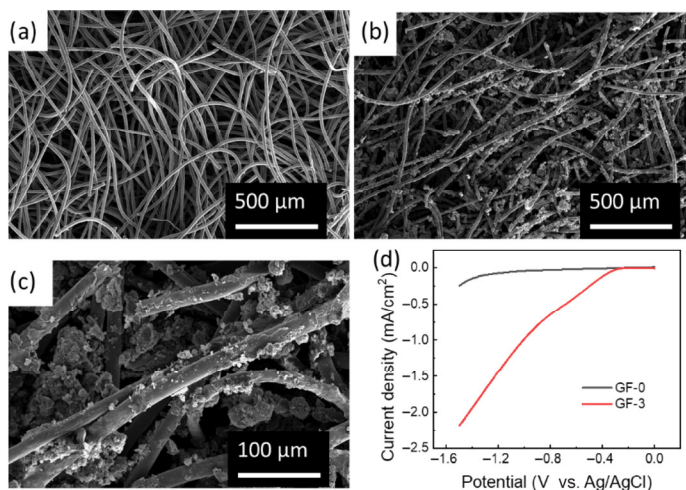

Figure 2 Characterization of cathode electrode. SEM images of the surface of (a) GF-0 and (b) and (c) GF-3. (d) LSV of GF-0, -3 ranging from 0 to −1.5 V using Ag/AgCl electrode as a reference. Conditions: scanning rate of 10 mV/s, 0.1 M NaCl neutral aqueous solution.

more hydrophobic and covers the active sites of porous carbon for electric conduction and H_2O_2 generation. GF-3 electrode possesses the best current response as the observed polarization curve (Fig. 2(d) and Fig. S4 in the ESM) among all cathodes according to LSV characterization, which indicates its ability of oxidation-reduction reaction for O_2 reduction towards H_2O_2 generation. The cathode screening was performed by electrochemical decolorization of RhB in NaCl solution under the catalysis of Fe^{2+} ions. The results in Figs. S5 and S7 in the ESM indicate the highest catalytic activity of GF-3 electrode among various electrodes.

Electro-generation of H_2O_2 in neutral solution by a DC power supply was carried out for the catalytic characterization of GF-3. As shown in Fig. 3(a), the accumulation rate increases with the applied current intensity ranging from 2 to 8 mA/cm^2. H_2O_2 electro-generation is a quasi-zero-order dynamic process. The dynamic constant is 1.44, 2.55, and 5.29 mg/(L·min) when the applied current intensity is 2, 4, and 8 mA/cm^2, respectively. It shows maximal Faraday current efficiency of 87% at the initial stage when applying the current of 8 mA/cm^2, then a steady efficiency of 60%–70% for the next 8 min (Fig. S8(a) in the ESM). Though H_2O_2 generation still exhibits an increasing tendency from 8 to 12 mA/cm^2, it is not so obvious anymore. Meanwhile, the current efficiency decreases. This decrease may be associated with the augmented polarization for the occurrence of side reactions, such as the evolution of hydrogen and self-decomposition of H_2O_2 [35, 36].

Usually acidic environment and extra O_2 are required for high-efficiency generation of H_2O_2 in EF process [25, 27, 35]. Follow-up treatment is needed to meet emission standards for this artificial circumstance. As a result, development of high-performance electrode for H_2O_2 generation in neutral solution and taking full advantage of the dissolved O_2 is most promising for EF application in polluted water treatment. Catalytic generation of H_2O_2 in solution with different pH values was performed to evaluate the activity of GF-3 (Fig. 3(b) and Fig. S8(b) in the ESM). GF-3 exhibits more active for H_2O_2 generation in neutral solution (pH 7: 5.3 mg/(L·min)) than in acid solution (pH 3: 2.1 mg/(L·min), pH 5: 3.5 mg/(L·min)), and even higher catalytic activity realized in the weak basic condition (pH 9: 5.8 mg/(L·min), pH 11: 6.3 mg/(L·min)). It also shows no significant difference on H_2O_2 generation with and without O_2 aeration in neutral condition (Fig. 3(c)). Thus, we deduce the H_2O_2 generation mechanism can be described as Eq. (1), in which a protonation
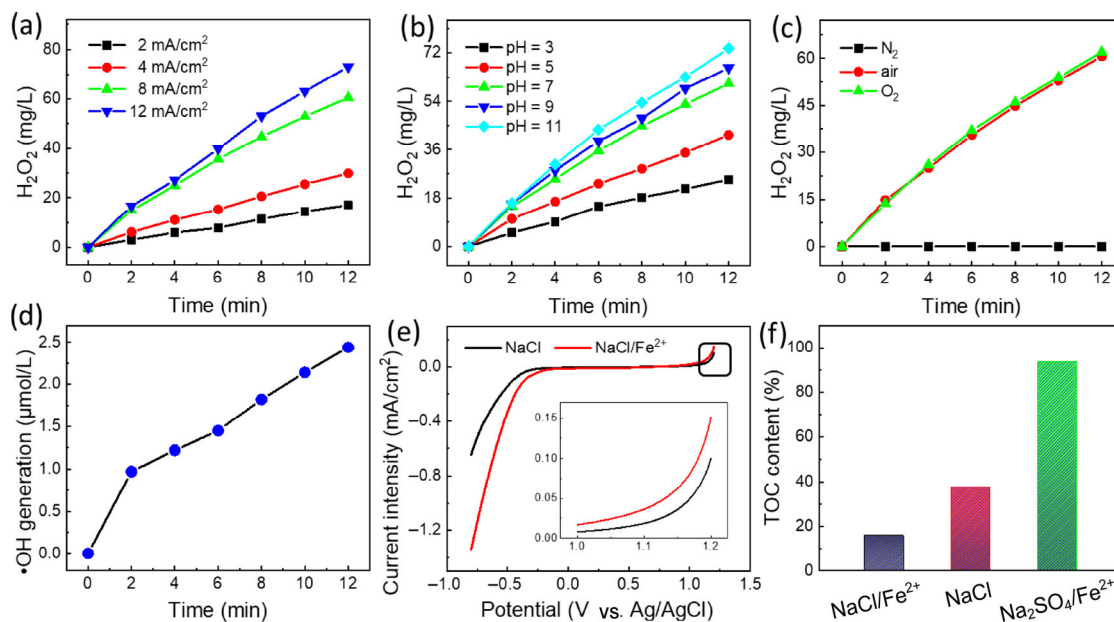
Figure 3 Electro-generation of H_2O_2 on GF-3 cathode (a) under different applying current intensities, (b) in solution with different pH values and (c) at different atmospheres. Conditions: (a) pH = 7, air; (b) 8 mA/cm^2, air; (c) pH = 7, 8 mA/cm^2. (d) Decomposing of H_2O_2 for ·OH generation under the catalysis of Fe^{2+} ions. Current intensity: 8 mA/cm^2, Fe^{2+} concentration: 0.01 M. (e) LSV in NaCl electrolyte solution with or without Fe^{2+} catalytic effect. (f) The comparison of remained TOC content within 75 s in different RhB solutions. 8 mA/cm^2, pH = 7, 50 mL RhB, 50 mg/L.

process of hydroperoxyl ion (HO_2^-) is subsequently brought in [37].

$$O_2 + H_2O + 2e^- \rightarrow HO_2^- + OH^- \qquad (1)$$
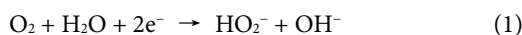
The generated H_2O_2 can efficiently decompose for •OH derivation under the catalysis of Fe^{2+} ions. Photoluminescence tests indicate the concentration of generated •OH can reach to 0.97 μmol/L (Fig. 3(d) and Fig. S9 in the ESM), then increases at a linear rate of 0.15 mg/(L·min). Besides, LSV spectrum obtained in NaCl/Fe^{2+} mixed electrolyte solution exhibits obvious enhanced polarization compared with that in NaCl solution (Fig. 3(e)). This suggests there is cooperation effect of H_2O_2 decomposition to •OH and active chlorine species existing, which may in favor of the degradation of organic components.

RhB was chosen as a simulated substrate for the succedent experimental demonstration for degrading organic compounds. It was surprising that it only took less than 1 min for the red solution to get transparent at a quasi-zero-order dynamic constant of 48 mg/(L·min) (Fig. S5(d) and Movie ESM1 in the ESM) and only 15.6% of TOC remained (Fig. 3(f)). For the case that only •OH exists without any active chlorine species generation (Fig. S10(a) in the ESM), it needs more than 20 min to remove RhB dye, and still 29.4% of TOC is remaining in solution. For the case that only active chlorine species exist without •OH generation (Fig. S10(b) in the ESM), the decolorization is even faster than the case of synthetically catalytic degradation in the first 30 s. However, the decolorization process is suspended after 30 s. The TOC removal efficiency (62.5%, Fig. 3(i)) after 75 s is rather lower than the case of synthetically catalytic degradation. In RhB degradation, N-demethylation and the destruction of the conjugated structure are two competitive processes. The conjugated structure of C=N and C=O structures make RhB showing the major absorption band at 554 nm. The generated chlorine species can rapidly attack the chromophore group, leading to the fast decolorization of RhB solution. However, the formed chloroderivatives byproducts in NaCl medium are recalcitrant, which hamper the further mineralization by chlorine species [38, 39]. •OH radicals can directly attack the central carbon of RhB, N-deethylation and cleavage chromophore intermediates [40]. Small molecules, such as formic acid and phthalic acid, are further formed via the open ring of aromatic fragments [40, 41]. These molecules

can be easily mineralized to be CO_2 and H_2O. Hence, the synthetically effect of fast decolorization by active chlorine species and deep mineralization by •OH is the most efficient choice for organic component degradation.

3.3 Construction and performance of SPECS

By integrating of the fabricated R-TENG as power supply and the above electrochemical cell for catalytic degradation of organic pollutants, a SPECS was constructed. The whole setup is schematically displayed in Fig. 4(a). The electric power output from the TENG directly determines the limit of molecule amount taking part into electrochemical reaction within a certain time. Though the TENG provides an ultrahigh voltage in open-circuit situation, the mismatching of the internal resistance of R-TENG and the apparent resistance of electrochemical cell can result in great decline of power output from TENG, which is a distinguished difference from the situation powered by a DC power supply [42, 43]. Thus, power management is needed for SPECS. Transformer was used for the aim of increasing current intensity in electrochemical system. Rectifier was used to change the alternating current (AC) output from R-TENG to DC for electrochemical reaction. After transformation, the peak V_{OC} dropped to 3 V and the peak I_{SC} increased to 0.6 mA (Fig. S11 in the ESM) at 1,400 rpm. Without power management (Fig. 4(b)), the voltage applied on electrochemical system was only 0.85 V, and the flowing current was 27 μA on average. After power management, the output power intensity was improved by 3.5 times. A voltage of 1.26 V and current of 60 μA on average could be employed to initiate the subsequent catalytic degradation reaction.

It is remarkable for organic contaminant degradation in the constructed SPECS, although the effect is not so excellent as that under the driven of DC power source. Figure 4(c) shows that 50 mL of RhB solution with a concentration of 4 mg/L can be thoroughly decolorized within 40 min after power management. As for a contrast in Fig. 4(d) and Fig. S12 in the ESM, after 70 min, there is still at least 10% RhB remained in solution without power management. According to some previous works [25, 31, 44], increased voltage from the unmanaged value to managed value will restrain the activity of electrochemical cell by increasing the probability of side reactions and the pH value of electrolyte solution. However, according to the
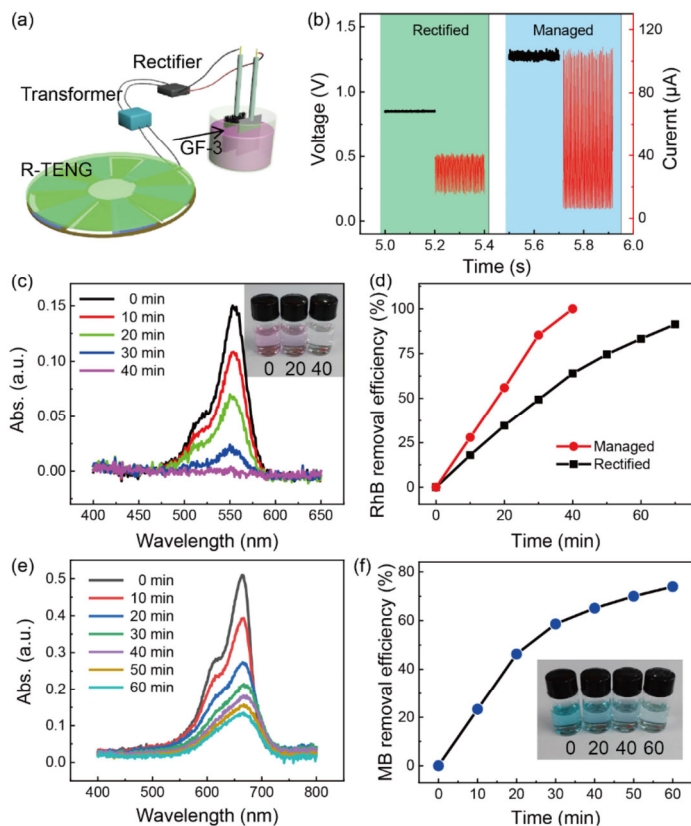
Figure 4 Setup and application of SPECS. (a) The setup of SPECS consisting of three main parts: R-TENG, circuit, electrochemical cell. A transformer and a rectifier are included in circuit. (b) The voltage applied on and current flowing through the electro-chemical cell without and with power management. Rectified means only rectifier was used to change the AC to DC. Absorption spectra of (c) RhB dye, (e) MB dye and removal efficiency of (d) RhB, (f) MB in SPECS as a function of time. Insert photos show the direct change of (c) RhB and (f) MB solution in visual at different periods. RhB: 50 mL, 4 mg/L; MB: 50 mL, 5 mg/L.

LSV results in Figs. 2(d) and 3(e) and electro-generation of H_2O_2 in Fig. 3(a), GF-3 cathode can still take full use of the injected electrons for O_2 reduction to generate H_2O_2. Meanwhile, Cl^- ions oxidation over Pt sheet anode for active chlorine generation is promoted. Besides, these electrochemical characterizations are based on the traditional DC power source, and the current intensity is related to power voltage, electrode resistance, bulk resistance, interface resistance of electrode and bulk solution. Though the voltage is raised to 1.26 from 0.85 V, the current flowed in the constructed SPECS is still dozens of microamperes. Cooperated reasons contribute to this phenomenon. The above SPECS provides a deep mineralization force for organic pollutants deconstruction, which is essentially different from the transformation from azo to quinoid compounds using a hybrid nanogenerator in another previous work [45]. This SPECS is also universal for the treatment of organic compounds, as the proof of MB degradation at a quasi-first-order kinetics rate of 0.023 min^{-1} evidenced in Figs. 4(e) and 4(f) and Fig. S13 in the ESM.

3.4 Application of SPECS for organic contaminant degradation

Furthermore, a WR-TENG was fabricated to replace the motor-driven R-TENG for the demo application of SPECS. Figure 5(a) exhibits a photo of the fabricated WR-TENG. The Cu-deposited disk-shape PCB with 32 intervals was used as the stator, while the FR4 glass fiber board adhered with PTFE film (100 μm in thickness) acted as the rotator. At the top of rotator shaft, a blade unit was fixed for wind energy harvesting. 21 nC of Q_{SC} (Fig. 5(b)), 50 V of V_{OC} (Fig. S14 in the ESM) and increasing peak I_{SC} (Fig. 5(c)) are
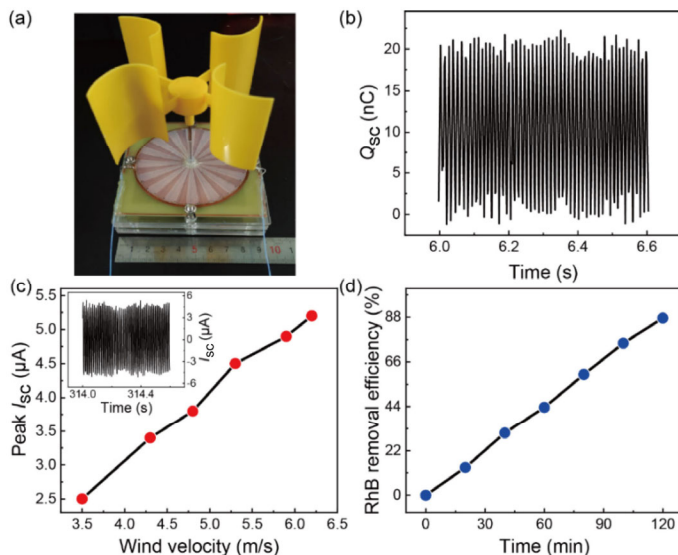

Figure 5 SPECS driven by WR-TENG. (a) A photo of WR-TENG for SPECS. (b) Q_{SC} of the WR-TENG when the wind speed was 6.2 m/s. (c) The peak I_{SC} of the WR-TENG at different wind speeds. The insert is the specific current output when the wind speed was 6.2 m/s. (d) Removal efficiency of RhB in SPECS powered by WR-TENG as a function of time. Wind speed: 6.2 m/s; RhB: 25 mL, 3 mg/L.

generated from the fabricated WR-TENG under the wind driven. By constructing the SPECS by integration of WR-TENG and the above electrochemical cell, RhB dye is degraded at a quasi-zero-order kinetics constant of 0.021 mg/(L·min), and a removal efficiency of 87.5% within 120 min (Fig. 5(d)) at the wind speed of 6.2 m/s. Despite this degradation effect is not so apparent as the condition driven by a motor in Figs. 4(c) and 4(d), the result is sufficient to prove the concept of SPECS for organic contaminant purification by harvesting distributed mechanical energy in environment.

4　Conclusions

In this work, a concept of SPECS for environmental remediation by harvesting distributed mechanical energy was proposed. The SPECS consists of three parts, including a R-TENG for electric power generation, an electrochemical cell for efficient active H_2O_2, •OH, chlorine species generation and organic compounds degradation, and power management unit for electric power optimization. By integrating the above components, the SPECS was constructed. After power management, the integrated R-TENG provides 3.5 times of electric power for the function of electrochemical cell. This SPECS can efficiently degrade RhB and MB in neutral condition without any O_2 aeration. Furthermore, a wind-driven SPECS demonstrates the potential application by harvesting wind energy for contaminant treatment. The proposed SPECS extends the application of TENGs in electrochemistry field, also offers guidelines for optimization of self-powered electrochemical reaction. More importantly, we provide a promising strategy based on the conversion from distributed mechanical energy to chemical energy for environmental remediation.

Acknowledgements

Electronic Supplementary Material: Supplementary material

(schematic charge transfer process for R-TENG, photographs and SEM images of GF-0, -3, LSV of GF-0, -1, -3, -5, Faraday current efficiency of GF-3 under different current intensities and in solution with different pH values, PL spectrum, absorption spectrum, V_{OC}, I_{SC} of the R-TENG after transformed, kinetic simulation of MB degradation and V_{OC} of the WR-TENG) is available in the online version of this article at https://doi.org/10.1007/s12274-019-2506-5.

References

[1] Fan, F. R.; Tian, Z. Q.; Wang, Z. L. Flexible triboelectric generator. *Nano Energy* **2012**, *1*, 328–334.

[2] Wang, Z. L. Nanogenerators, self-powered systems, blue energy, piezotronics and piezo-phototronics—A recall on the original thoughts for coining these fields. *Nano Energy* **2018**, *54*, 477–483.

[3] Wang, Z. L. Triboelectric nanogenerators as new energy technology and self-powered sensors—Principles, problems and perspectives. *Faraday Discuss.* **2014**, *176*, 447–458.

[4] Wu, C. S.; Wang, A. C.; Ding, W. B.; Guo, H. Y.; Wang, Z. L. Triboelectric nanogenerator: A foundation of the energy for the new era. *Adv. Energy Mater.* **2019**, *9*, 1802906.

[5] Wang, Z. L. On Maxwell's displacement current for energy and sensors: The origin of nanogenerators. *Mater. Today* **2017**, *20*, 74–82.

[6] Shao, J. J.; Willatzen, M.; Jiang, T.; Tang, W.; Chen, X. Y.; Wang, J.; Wang, Z. L. Quantifying the power output and structural figure-of-merits of triboelectric nanogenerators in a charging system starting from the Maxwell's displacement current. *Nano Energy* **2019**, *59*, 380–389.

[7] Liu, W. L.; Wang, Z.; Wang, G.; Liu, G. L.; Chen, J.; Pu, X. J.; Xi, Y.; Wang, X.; Guo, H. Y.; Hu, C. G. et al. Integrated charge excitation triboelectric nanogenerator. *Nat. Commun.* **2019**, *10*, 1426.

[8] Liang, X.; Jiang, T.; Liu, G. X.; Xiao, T. X.; Xu, L.; Li, W.; Xi, F. B.; Zhang, C.; Wang, Z. L. Triboelectric nanogenerator networks integrated with power management module for water wave energy harvesting. *Adv. Funct. Mater.* **2019**, *29*, 1807241.

[9] Zhang, C.; Wang, Z. L. Tribotronics—A new field by coupling triboelectricity and semiconductor. *Nano Today* **2016**, *11*, 521–536.

[10] Yin, W. L.; Xie, Y. D.; Long, J.; Zhao, P. F.; Chen, J. K.; Luo, J. K.; Wang, X. Z.; Dong, S. R. A self-power-transmission and non-contact-reception keyboard based on a novel resonant triboelectric nanogenerator (R-TENG). *Nano Energy* **2018**, *50*, 16–24.

[11] Zhou, C. J.; Yang, Y. Q.; Sun, N.; Wen, Z.; Cheng, P.; Xie, X. K.; Shao, H. Y.; Shen, Q. Q.; Chen, X. P.; Liu, Y. N. et al. Flexible self-charging power units for portable electronics based on folded carbon paper. *Nano Res.* **2018**, *11*, 4313–4322.

[12] Liu, Z. R.; Nie, J. H.; Miao, B.; Li, J. D.; Cui, Y. B.; Wang, S.; Zhang, X. D.; Zhao, G. R.; Deng, Y. B.; Wu, Y. H. et al. Self-powered intracellular drug delivery by a biomechanical energy-driven triboelectric nanogenerator. *Adv. Mater.* **2019**, *31*, 1807795.

[13] Gao, S. Y.; Wang, M.; Chen, Y.; Tian, M.; Zhu, Y. Z.; Wei, X. J.; Jiang, T. An advanced electro-Fenton degradation system with triboelectric nanogenerator as electric supply and biomass-derived carbon materials as cathode catalyst. *Nano Energy* **2018**, *45*, 21–27.

[14] Cui, S. W.; Zheng, Y. B.; Liang, J.; Wang, D. A. Triboelectrification based on double-layered polyaniline nanofibers for self-powered cathodic protection driven by wind. *Nano Res.* **2018**, *11*, 1873–1882.

[15] Yeh, M. H.; Guo, H. Y.; Lin, L.; Wen, Z.; Li, Z. L.; Hu, C. G.; Wang, Z. L. Rolling friction enhanced free-standing triboelectric nanogenerators and their applications in self-powered electrochemical recovery systems. *Adv. Funct. Mater.* **2016**, *26*, 1054–1062.

[16] Chen, S. W.; Wang, N.; Ma, L.; Li, T.; Willander, M.; Jie, Y.; Cao, X.; Wang, Z. L. Triboelectric nanogenerator for sustainable wastewater treatment via a self-powered electrochemical process. *Adv. Energy Mater.* **2016**, *6*, 1501778.

[17] Tang, W.; Han, Y.; Han, C. B.; Gao, C. Z.; Cao, X.; Wang, Z. L. Self-powered water splitting using flowing kinetic energy. *Adv. Mater.* **2015**, *27*, 272–276.

[18] Su, Y. J.; Yang, Y.; Zhang, H. L.; Xie, Y. N.; Wu, Z. M.; Jiang, Y. D.; Fukata, N.; Bando, Y.; Wang, Z. L. Enhanced photodegradation of methyl orange with TiO₂ nanoparticles using a triboelectric nanogenerator. *Nanotechnology*

[19] Yu, X.; Han, X.; Zhao, Z. H.; Zhang, J.; Guo, W. B.; Pan, C. F.; Li, A. X.; Liu, H.; Wang, Z. L. Hierarchical TiO₂ nanowire/graphite fiber photoelectrocatalysis setup powered by a wind-driven nanogenerator: A highly efficient photoelectrocatalytic device entirely based on renewable energy. *Nano Energy* **2015**, *11*, 19–27.

[20] Wei, A. M.; Xie, X. K.; Wen, Z.; Zheng, H. C.; Lan, H. W.; Shao, H. Y.; Sun, X. H.; Zhong, J.; Lee, S. T. Triboelectric nanogenerator driven self-powered photoelectrochemical water splitting based on hematite photoanodes. *ACS Nano* **2018**, *12*, 8625–8632.

[21] Feng, Y. W.; Ling, L. L.; Nie, J. H.; Han, K.; Chen, X. Y.; Bian, Z. F.; Li, H. X.; Wang, Z. L. Self-powered electrostatic filter with enhanced photocatalytic degradation of formaldehyde based on built-in triboelectric nanogenerators. *ACS Nano* **2017**, *11*, 12411–12418.

[22] Liu, W. X.; Wu, J. Y.; He, W.; Xu, F. L. A review on perfluoroalkyl acids studies: Environmental behaviors, toxic effects, and ecological and health risks. *Ecosyst. Health Sustain.* **2019**, *5*, 1–19.

[23] Deng, W. J.; Li, N.; Ying, G. G. Antibiotic distribution, risk assessment, and microbial diversity in river water and sediment in Hong Kong. *Environ. Geochem. Health* **2018**, *40*, 2191–2203.

[24] Dominguez, C. M.; Oturan, N.; Romero, A.; Santos, A.; Oturan, M. A. Optimization of electro-Fenton process for effective degradation of organochlorine pesticide lindane. *Catal. Today* **2018**, *313*, 196–202.

[25] Zhou, M. H.; Yu, Q. H.; Lei, L. C.; Barton, G. Electro-Fenton method for the removal of methyl red in an efficient electrochemical system. *Sep. Purif. Technol.* **2007**, *57*, 380–387.

[26] An, S. F.; Zhang, G. H.; Wang, T. W.; Zhang, W. N.; Li, K. Y.; Song, C. S.; Miller, J. T.; Miao, S.; Wang, J. H.; Guo, X. W. High-density ultra-small clusters and single-atom fe sites embedded in graphitic carbon nitride (g-C₃N₄) for highly efficient catalytic advanced oxidation processes. *ACS Nano* **2018**, *12*, 9441–9450.

[27] Zhang, Z. H.; Meng, H. S.; Wang, Y. J.; Shi, L. M.; Wang, X.; Chai, S. N. Fabrication of graphene@graphite-based gas diffusion electrode for improving H₂O₂ generation in electro-Fenton process. *Electrochim. Acta* **2018**, *260*, 112–120.

[28] Schwarz, H. A.; Dodson, R. W. Equilibrium between hydroxyl radicals and thallium (II) and the oxidation potential of hydroxyl(aq). *J. Phys. Chem.* **1984**, *88*, 3643–3647.

[29] Rositano, J.; Nicholson, B. C.; Pieronne, P. Destruction of cyanobacterial toxins by ozone. *Ozone: Sci. Eng.* **1998**, *20*, 223–238.

[30] Szpyrkowicz, L.; Kaul, S. N.; Neti, R. N.; Satyanarayan, S. Influence of anode material on electrochemical oxidation for the treatment of tannery wastewater. *Water Res.* **2005**, *39*, 1601–1613.

[31] Ma, X. J.; Zhou, M. H. A comparative study of azo dye decolorization by electro-Fenton in two common electrolytes. *J. Chem. Technol. Biotechnol.* **2009**, *84*, 1544–1549.

[32] Yu, F. K.; Zhou, M. H.; Yu, X. M. Cost-effective electro-Fenton using modified graphite felt that dramatically enhanced on H₂O₂ electro-generation without external aeration. *Electrochim. Acta* **2015**, *163*, 182–189.

[33] Sellers, R. M. Spectrophotometric determination of hydrogen peroxide using potassium titanium(IV) oxalate. *Analyst* **1980**, *105*, 950–954.

[34] Barreto, J. C.; Smith, G. S.; Strobel, N. H. P.; McQuillin, P. A.; Miller, T. A. Terephthalic acid: A dosimeter for the detection of hydroxyl radicals *in vitro*. *Life Sci.*, **1995**, *56*, PL89–PL96.

[35] Wen, S. L.; Niu, Z. Y.; Zhang, Z.; Li, L. H.; Chen, Y. C. *In-situ* synthesis of 3D GA on titanium wire as a binder-free electrode for electro-Fenton removing of EDTA-Ni. *J. Hazard. Mater.* **2018**, *341*, 128–137.

[36] Wang, Y.; Liu, Y. H.; Liu, T. F.; Song, S. Q.; Gui, X. C.; Liu, H.; Tsiakaras, P. Dimethyl phthalate degradation at novel and efficient electro-Fenton cathode. *Appl. Catal., B* **2014**, *156*, 1–7.

[37] Agladze, G. R.; Tsurtsumia, G. S.; Jung, B. I.; Kim, J. S.; Gorelishvili, G. Comparative study of hydrogen peroxide electro-generation on gas-diffusion electrodes in undivided and membrane cells. *J. Appl. Electrochem.* **2007**, *37*, 375–383.

[38] de Araújo, D. M.; Cotillas, S.; Sáez, C.; Cañizares, P.; Martínez-Huitle, C. A.; Rodrigo, M. A. Activation by light irradiation of oxidants electrochemically generated during Rhodamine B elimination. *J. Electroanal. Chem.* **2015**, *757*, 144–149.

2013, *24*, 295401.

[39] Thiam, A.; Salazar, R.; Brillas, E.; Sirés, I. Electrochemical advanced oxidation of carbofuran in aqueous sulfate and/or chloride media using a flow cell with a RuO_2-based anode and an air-diffusion cathode at pre-pilot scale. *Chem. Eng. J.* **2018**, *335*, 133–144.

[40] Yu, K.; Yang, S. G.; He, H.; Sun, C.; Gu, C. G.; Ju, Y. M. Visible light-driven photocatalytic degradation of rhodamine B over $NaBiO_3$: Pathways and mechanism. *J. Phys. Chem. A* **2009**, 113, 10024–10032.

[41] Fu, H. B.; Zhang, S. C.; Xu, T. G.; Zhu, Y. F.; Chen, J. M. Photocatalytic degradation of rhb by fluorinated Bi_2WO_6 and distributions of the intermediate products. *Environ. Sci. Technol.* **2008**, *42*, 2085–2091.

[42] Chen, Y.; Wang, M.; Tian, M.; Zhu, Y. Z.; Wei, X. J.; Jiang, T.; Gao, S. Y. An innovative electro-Fenton degradation system self-powered by triboelectric nanogenerator using biomass-derived carbon materials as cathode catalyst. *Nano Energy* **2017**, *42*, 314–321.

[43] Qin, H. F.; Cheng, G.; Zi, Y. L.; Gu, G. Q.; Zhang, B.; Shang, W. Y.; Yang, F.; Yang, J. J.; Du, Z. L.; Wang, Z. L. High energy storage efficiency triboelectric nanogenerators with unidirectional switches and passive power management circuits. *Adv. Funct. Mater.* **2018**, *28*, 1805216.

[44] Li, X. H.; Jin, X. D.; Zhao, N. N.; Angelidaki, I.; Zhang, Y. F. Efficient treatment of aniline containing wastewater in bipolar membrane microbial electrolysis cell-Fenton system. *Water Res.* **2017**, *119*, 67–72.

[45] Yang, Y.; Zhang, H. L.; Lee, S.; Kim, D.; Hwang, W.; Wang, Z. L. Hybrid energy cell for degradation of methyl orange by self-powered electrocatalytic oxidation. *Nano Lett.* **2013**, *13*, 803–808.